

The Physico-Chemical Characterization of Mesoporous Sulfated Zirconia Nanoparticles Prepared under Structure-Directing-Free for *n*-Hexane Isomerization

Gongyi Guo^{1*}, Yuli Chen², Shi Xu³

¹School of Materials Science and Engineering, Shanghai Jiao Tong University, Shanghai, China

²College of Environmental and Chemical Engineering, Shanghai University, Shanghai, China

³Instrumental Analysis Center, Shanghai Jiao Tong University, Shanghai, China

Email: *guo_gongyi@hotmail.com

How to cite this paper: Guo, G.Y., Chen, Y.L. and Xu, S. (2020) The Physico-Chemical Characterization of Mesoporous Sulfated Zirconia Nanoparticles Prepared under Structure-Directing-Free for *n*-Hexane Isomerization. *Journal of Minerals and Materials Characterization and Engineering*, 8, 59-83.

<https://doi.org/10.4236/jmmce.2020.83005>

Received: January 9, 2020

Accepted: April 13, 2020

Published: April 16, 2020

Copyright © 2020 by author(s) and Scientific Research Publishing Inc.

This work is licensed under the Creative Commons Attribution International License (CC BY 4.0).

<http://creativecommons.org/licenses/by/4.0/>



Open Access

Abstract

This article describes the physico-chemical characterization of the sulfated zirconia catalysts prepared from zirconyl chloride, acetic acid and ammonium persulfate system under structure-directing-free and calcined at 650°C. The catalysts were characterized via an array of characterization techniques such as surface acidity and texture measurements, X-ray diffraction (XRD), ultraviolet-visible spectroscopy (UV-VIS), scanning electron microscopy (SEM) equipped with energy dispersive X-ray spectroscopy (EDXS), high resolution transmission electron microscopy (HRTEM), X-ray photoelectron spectroscopy (XPS), infrared spectroscopy (IR), thermogravimetric measurement (TG) coupled with a quadrupole mass spectrometer (MS), inductively coupled plasma-atomic emission spectroscopy (ICP-AES) and/or mass spectrometry (ICP-MS). It is clear from TG-MS, ICP-AES, and IR analyses that the precursor of the catalyst is a sulphur species-doped zirconium oxy-hydroxyl acetate complex. The presence of zirconium-bound sulfate groups results in the superacidity of the catalyst and hence high activity in *n*-hexane isomerization. It is shown from nitrogen adsorption and desorption, FESEM, and HRTEM measurements that the materials exhibit mesoporous and nanocrystalline structure.

Keywords

Physico-Chemical Characterization, Mesoporous, Nanoparticle, Sulfated Zirconia, *n*-Hexane Isomerization

1. Introduction

High surface area, nanostructured, crystalline metal oxides are a very interesting class of materials due to their great potential in various applications [1]. Environmental concerns have promoted legislation to limit the amount of aromatics in gasoline. However, reduction of aromatics has a negative impact on gasoline octane number that has to be compensated by other approaches. Alkanes are environmentally more acceptable than aromatics, and the branched hydrocarbons have higher octane numbers than linear alkane. The octane numbers are 26 and 93 for *n*-hexane and 2,2-dimethylbutane, respectively. The skeletal isomerization of *n*-alkanes plays an important role in the production of branched, high-octane hydrocarbons as a replacement of traditional tetra-ethyl lead additives. Isomerization of normal hexane (*n*-C₆) has been recognized to be one of the most economical units to boost octane level especially for the lower boiling gasoline. The process is typically catalyzed by bifunctional Pt/H-mordenite catalysts [2]. Recently, zirconia has been reported as a popular support for various reactions because of its high thermal stability, acid-base properties, and redox surface properties. As for supported catalysts, the catalytic activity is greatly dependent on the morphology, porosity, and surface area of the catalyst support. In our work, mesoporous monometallic Pd-promoted sulfated zirconia was used for *n*-hexane isomerization [3]. Herein, we describe the physico-chemical characterization of the sulfated zirconia catalysts prepared from zirconyl chloride, acetic acid and ammonium persulfate system under structure-directing-free and calcined at 650 °C, showing their high acidity, mesoporous and nanocrystalline structure.

2. Experimental

Details of the material preparation have been reported elsewhere by the authors [3]. In the present article, the materials were examined via an array of characterization techniques, as mentioned above, for a complete chemical and structural description.

X-ray diffraction (XRD) data were collected by using Bruker-AXS D8 Advance diffractometer or Rigaku D/max-2550/pc XRD. The XRD pattern was recorded by scanning it over a 2θ range of 20° - 90° at a scan speed of 0.2 s/step with an increment 0.02°/step and utilizing CuK_α radiation at 40 kV and 40 mA. The identification of monoclinic (M), tetragonal (T) zirconia, zircosulfate and palladium sulfate was accomplished by comparison of the XRD data to the Powder Diffraction File (file numbers 37-1484, 79-1771 and 01-079-1763, 008-0495 and 01-0366, and 01-083-0469, respectively), using the Bruker Eva.exe program. The mean crystallite size was determined by applying the well-known Scherrer equation or Rietveld method.

The diffused reflectance UV-Vis spectra of the sulfated zirconia were recorded on a Varian Cary 5000 UV-VIS-NIR spectrophotometer equipped with an integrating sphere attachment. The computer processing of the absorption spectrum was done with Cary I-E software that allowed calculation of the Kubelka-Munk

function $F(R)$ from the absorbance data. The band gap energy (E_g) for an allowed transition was determined by finding the intercept of the straight line in a plot of $[F(R) \times h\nu]^2$ versus $h\nu$, where $h\nu$ is the incident photon energy. Or, the absorption edge energy was determined for the spectrum by a linear extrapolation to zero absorption.

Scanning electron microscopy (SEM) images were captured with a Nova Nano SEM 230 field-emission microscope operated at 30 KV. Energy dispersive X-ray (EDX) analyses were performed using X-MAX 80 EDS on Nova Nano SEM 230. Samples for SEM were dusted on an adhesive conductive carbon disk attached to an aluminium mount.

TEM observations were performed in an instrument equipped with a field-emission gun operating at 200 KV (JEOL-2100F) and a point-to-point resolution of 2.3 Å. High-resolution TEM micrographs were recorded using a slow scan CCD camera. The sample powders were sonicated for 5 min in absolute ethanol. A drop of the resulting suspension was then put on a carbon-coated copper grid and dried at room temperature prior to the measurement. The dimensions of the particles were measured from micrographs, taken with a transmission electron microscope.

XPS analysis was performed on a Kratos Axis Ultra^{DLD} spectrometer (Kratos Analytical, Manchester, UK) equipped with a monochromatized aluminum X-ray source (powered at 10 mA and 15 kV) and an eight channeltron detector at room temperature under ca. 10^{-6} Pa vacuum. Powder samples were pressed on indium supports to provide a flat surface and decrease charging effect. The pass energy was set at 160 eV for the survey scan and 40 eV for individual spectra. The scan was conducted with a step size of 0.1 eV. Binding energy (BE) calibration was based on C1s at 284.6 eV. The acquired spectra were fitted using the Levenberg-Marquardt optimization algorithm, and peak shapes were modelled using an asymmetric Lorentzian line shape convolved with a Gaussian function, using the CACA-XPS processing software. The $I(\text{Zr}3d_{5/2})/I(\text{Zr}3d_{3/2})$ intensity ratio was fixed at 1.5 with an energy difference of 2.43 eV, which is in agreement with the handbook [4].

Fourier-transform infrared spectra for the pristine complex and catalysts were recorded on a Nicolet 6700 FTIR spectrophotometer (Thermo Scientific) in wavenumber 4000 - 400 cm^{-1} range, with a resolution of 4 cm^{-1} and a scan number of 16. The infrared spectra of samples were studied as powder dispersed in a KBr pellet.

The thermogravimetric (TG) measurement was coupled with a quadrupole mass spectrometer (MS) to identify the species evolved from the sample during the thermogravimetric experiment, *i.e.*, calcination process, and thus to better explain the catalytic behaviour of our sample. The measurement mode used in our work was multiple ion detection (MID), it is possible to scan only selected ions. The time dwelled at a given ion with MID mode may be much longer than with a full scanning method, thus improving its selectivity. The signals for masses 17 (NH_3^+), 18 (H_2O^+), 30 (NO^+), 31 (CH_3O^+), 43 (CH_3CO^+), 44 (CO_2^+), 46

(NO₂⁺), 48 (SO⁺), 64 (SO₂⁺), 80 (SO₃⁺) were recorded. The residual mass after 700 °C was considered as inorganic solids.

Zirconium and other metals, carbon and sulphur, and chlorine in samples were determined by inductively coupled plasma-atomic emission spectroscopy (ICP-AES) or mass spectrometry (ICP-MS) [Thermo Scientific iCAP 6000 series ICP Spectrometer] and energy dispersive X-ray spectroscopy (EDXS) on scanning electron microscopy (SEM), elemental analysis [Elementar Vario ELIII], and X-ray fluorescence analysis, respectively.

3. Results and Discussion

3.1. Acidity

Acidity is the most important function of sulfated zirconia and it is evidently connected to the presence of sulfate groups binding with zirconia surface in an inorganic chelating bidentate fashion, because zirconia itself exhibits only weak acidic properties. Zr⁴⁺ ion has a small radius of 0.84 Å and can act as Lewis acid site. Sulfate group is electron-withdrawing from zirconia support and the Lewis acidity is, therefore, created on zirconia or strengthened, in other words, the Lewis acid sites are coordinatively deficient Zr (IV) centre promoted by the electron-withdrawing neighbouring sulfate group. Brønsted acid sites are recognized as being surface hydroxyls [5]. Brønsted acidity could occur from “hydrated” polymeric sulfate species (surface pyrosulfate species), in other words, the Brønsted acid sites result from the weakening of the O-H bond by the neighbouring sulfate group. When the sulfate ions are incorporated into zirconium hydroxyl compounds, they must link hydroxyl ions. Terminal hydroxyls (t-OH) are hydroxyl groups bound to a metal centre (M-OH). They act as a Brønsted base, reacting with acidic molecules. Bridging hydroxyl (b-OH) groups are protons bound to oxygen atoms that connect two or more metal atoms [M-(OH)-M] and act as Brønsted acid sites. Both bridging and terminal hydroxyl groups co-exist in both zirconium hydroxyl compounds and crystalline zirconia. It is, therefore, clear that the most acid sites are in line with the fact that a catalyst has great sulfate content. The increased sulfate groups not only favour stabilizing the active tetragonal phase of zirconia but also increasing the total surface area and pore volume, and hence enhancing the Brønsted and Lewis acidities, and increasing the oxidative dehydrogenation. The high acidity of the sulfated zirconia support could explain the small metal particle size (as will be corroborated later by the FETEM observations), since the presence of acidic groups increases the hydrophilic character of the support and favors the diffusion of the metal precursor [6].

Pyridine is widely used to identify the concentration and nature of acid sites on the surface of sulfated zirconia. The interaction of pyridine nitrogen with acidic sites gives rise to two different frequencies of bending vibration. Adsorption of pyridine on Brønsted acid sites forms a pyridinium ion, giving rise to infrared bands at ca. 1540, 1611, and 1638 cm⁻¹; pyridine adsorption on Lewis

acid sites yields covalently bound species, giving characteristic bands at ca. 1445, 1480 and 1575 cm^{-1} . The band around 1486 cm^{-1} is attributed to a combination band associated with both Brønsted and Lewis acid sites.

It is evident that the band area calculated from the integrated IR bands attributed to Brønsted and Lewis acid sites indicates the strength of Brønsted and Lewis acidities. It may be noted from **Table 1** and **Table 2** that with increasing temperature from room temperature to 300 °C, which is higher than the temperature required for hydrocarbon hydroisomerization reaction, the Brønsted and Lewis acidities of the catalysts studied remain with considerable intensity. In addition, it is worth pointing out that the typical Brønsted acidities (1540 and 1638 cm^{-1}) for the monometallic Pd-promoted sulfated zirconia (**Table 2**) can be interestingly strengthened by raising temperature, leading to a high catalytic activity in *n*-hexane isomerization.

3.2. Texture

Besides the acidity, the textural parameters such as specific surface area, pore diameter and volume of a catalyst also contribute to the catalyst activity. A higher specific surface area favours the spacing of the sulfate groups, leading to less dense, more accessible and a large number of total acid sites. The large pore diameter and volume can make the reaction more feasible due to easy diffusion of reactants and product molecules. The textural properties of a catalyst are largely determined by preparation method including the initial precursor used as well as the post-synthesis treatment, e.g., digestion, calcination temperature, and

Table 1. Acidities of the sulfated zirconia prepared by the present method.

Desorp.	1638 cm^{-1}	1608 cm^{-1}	1575 cm^{-1}	1540 cm^{-1}	1489 cm^{-1}	1443 cm^{-1}
temp. °C	I.A. (B)	I.A. (B)	I.A. (L)	I.A. (B)	I.A. (B + L)	I.A. (L)
RT	0.615	6.032	0.474	1.407	4.402	6.404
100	0.634	6.090	0.488	1.457	3.866	6.190
200	0.495	5.412	0.299	1.119	2.029	5.125
300	0.273	4.513	0.180	0.650	1.283	3.965

B—Brønsted acid, L—Lewis acid, I.A.—Integrated area, RT—room temperature, Desorp.—Desorption.

Table 2. Acidities of the monometallic Pd-promoted sulfated zirconia prepared by the present method.

Desorp.	1638 cm^{-1}	1608 cm^{-1}	1575 cm^{-1}	1540 cm^{-1}	1489 cm^{-1}	1443 cm^{-1}
Temp. °C	I.A. (B)	I.A. (B)	I.A. (L)	I.A. (B)	I.A. (B + L)	I.A. (L)
RT	0.410	1.543	0.252	1.456	1.564	2.121
100	0.502	1.598	0.069	1.719	1.634	1.648
200	0.584	1.506	/	1.825	1.614	0.990
300	0.645	1.267	/	1.787	1.440	0.784

B—Brønsted, L—Lewis, I.A.—Integrated area, Desorp.—Desorption, RT—Room temperature.

impregnation. The catalytic properties of sulfated metal oxides depend strongly on subtle variation in the material. The preparation method determines the dispersion and nature of sulphur species on the surface. Usually, sulfated zirconia is prepared by first precipitating the hydroxide of zirconium which, after washing and drying, is treated with a solution of sulfuric acid or ammonium sulfate and followed by calcination. The initial precursor used for preparing sulfated zirconia plays a vital role in the final texture and performance of a catalyst. Use of various precursors alters both Lewis and Brønsted acidity substantially. The most frequently used precursor for sulfation is dilute sulfuric acid and ammonium sulfate. The sulfation treatment of amorphous zirconium hydroxide not only provides superacid sites but also creates reducible sulfate sites [7]. The conventional preparation method for sulfated zirconia (SZ) results in microporous material. The synthesis of mesoporous zirconia has been advanced largely by utilizing templates or surfactants [1]. In our work, however, mesoporous sulfated zirconia nanoparticles have been prepared under structure-directing-free at 650 °C from zirconyl chloride, acetic acid and ammonium persulfate system. **Figure 1(a)** and **Figure 1(c)** present nitrogen adsorption and desorption isotherms at 77 K for the sulfated zirconia and monometallic Pd-promoted sulfated zirconia, respectively. The shape and sharpness of the isotherm reveal the mesoporous feature of the catalyst. According to the IUPAC classification [8], the shape of the isotherm resembles the type IV isotherm with H_1 hysteresis loop at high relative pressure, which is a characteristic of the mesoporous material, indicating capillary condensation taking place in mesopores [1] [9]. Pronounced desorption hysteresis present in the isotherm is an indicative of the presence of large mesopores in the material.

The sulfated zirconia has a bimodal pore diameter distribution in the mesoporous range, the one between 6 and 58 nm is the major, along with minor at the diameter range around 4 nm, as shown in the BJH pore distribution **Figure 1(b)**. The monometallic Pd-promoted sulfated zirconia only has a pore diameter distribution in the mesoporous range (5 to 58 nm), as shown in the BJH pore distribution **Figure 1(d)**.

We used a mesoporous zirconium oxy-hydroxy acetate-persulfate complex synthesised from the zirconyl chloride, acetic acid and ammonium persulfate system as a precursor of the sulfated zirconia studied. In the complex the high valence of Zr^{+4} and large Zr^{+4} -O bond polarization can lead to a strong bonding between Zr^{+4} and carboxylate oxygens, facilitating the synthesis of the complex with high surface areas, thermal and chemical stability [10] [11] [12] [13]. Ammonium persulfate is used for the precursor of sulfation, yielding a sufficient number of both Lewis and Brønsted types of acidity, as shown in **Table 1** and **Table 2**. Furthermore, the activity for alkane isomerization is correlated to the surface site density of sulfates, and the higher the surface sulfate coverage the higher the initial isomerization activity of sulfated zirconia, thereby showing the importance of persulfates for the initiation of the reaction.

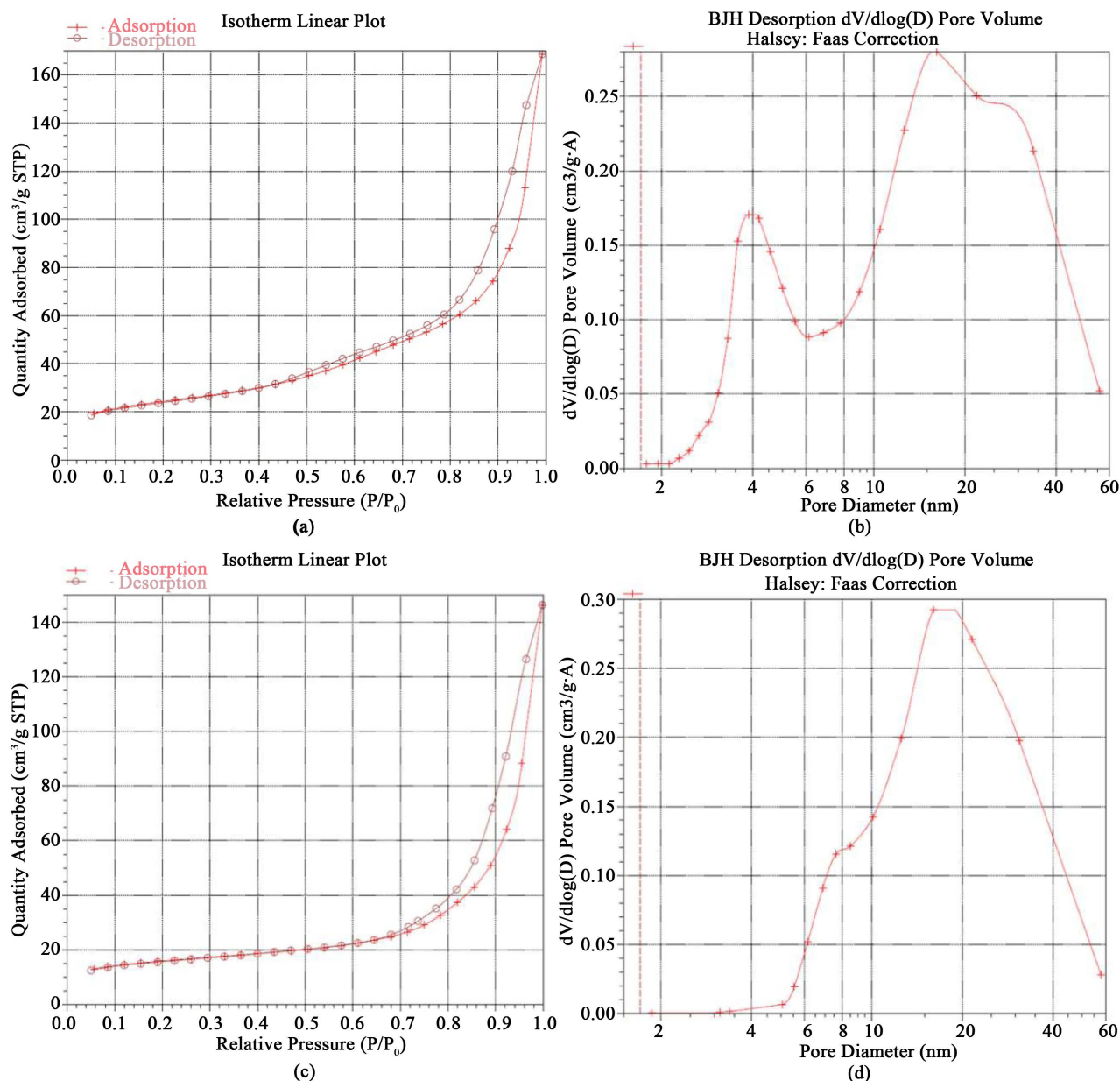


Figure 1. Nitrogen adsorption-desorption isotherms and corresponding pore size distributions of the sulfated zirconia ((a), (b)) and the monometallic Pd-promoted sulfated zirconia ((c), (d)).

In addition to the initial precursor used, digestion, calcination temperature and impregnation have important effect on the texture properties of a catalyst. The process of digestion in the course of preparation leads to an extensive polymerization through the condensation of the hydroxyl groups in the hydrous zirconium acetate complex to form ordered three-dimensional porous structure. The catalytic performance of sulfated zirconia hinges upon the successful incorporation of sulphony functional groups into the zirconia framework. The presence of acetic acid in solution with sulfuric acid favours a higher sulphur content in the sample. The increase in the sulphur content favours the formation of some complex sulfates that could exhibit both Brønsted and Lewis acidities. The

increased surface area may be due to the presence of bridging sulfate SO_4^{2-} ions on the surface. The bridging sulfate ions replace hydroxyl species on the surface, resulting in a more rigid and stable structure. Furthermore, it has been reported that the bridging sulfate ions elongate the Zr-Zr separation from about 3.4 - 4.3 Å, which facilitates the dispersion of oxide particles and accordingly, increases the surface area.

It is well known that the specific surface area decreases as the calcination temperature increases and the mean pore size follows the opposite trend. This is because of the crystallite growth and pore wall thickening. It is, however, worth pointing out that our sulfated zirconia samples were prepared at calcination temperature as high as 650 °C, still showing a high BET surface area ($83 \text{ m}^2\cdot\text{g}^{-1}$), mesopore (18 nm), and large total pore volume ($0.42 \text{ cm}^3\cdot\text{g}^{-1}$), as shown in **Table 3**. Compared to the properties of the recently published sulfated zirconia and other types of acid catalysts for *n*-hexane isomerization, it may be clear from **Table 3** that the sulfated zirconia studied shows the best performance among different types of acid catalysts. The mesoporous sulfated zirconia was used for *n*-hexane isomerization, resulting in a high catalytic activity [3].

A higher sulphur content in the sulfated zirconia made the active tetragonal crystalline phase of zirconia to be stabilised by a contribution to the rigidity of

Table 3. Comparison of the experimental conditions and results of recent studies with our work for mesoporous sulfated zirconia.

Catalyst	Preparation conditions				Textural Properties			Ref.	
	Template	Surfactant	Temp. [°C]	S [wt%]	Metal [wt%]	Surface area [$\text{m}^2\cdot\text{g}^{-1}$]	Pore size [nm]		Pore Vol. [$\text{cm}^3\cdot\text{g}^{-1}$]
Mesoporous ZrO_2 nanoframes	yes	no	550		Ni 10	68.8	3.8		[17]
micro-meso Pt/H MOR/9.5 (mordenite zeolites)	yes		550		Pt 1.5	114	13	0.25	[2]
Pd-Pt Supported on sulfated zirconia			600 - 450	1.3	Pd + Pt 0.5	115		0.175	[6]
MOF-Derived Tungstated Zirconia	yes	no	650		W 12.2	50		0.1	[18]
SZ	no	no	650	1.29		83	18	0.42	our work
Pd-SZ	no	no	650 - 450	2.38	Pd 0.43	91	12	0.26	our work
Spent Pd-SZ	no	no	650 - 450	1.44	Pd 0.55	89.2	10.5	0.26	our work

the structure, leading to an elongation of the Zr-Zr bond distance, or by retarding the tetragonal-to-monoclinic transformation. As temperature increased, more crystalline tetragonal phases were developed without the appearance of the monoclinic phase until about 650°C, as shown in **Figure 2**.

The organic components present in the zirconium oxy-hydroxy acetate-persulfate complex were partially or completely removed at high temperature, leading to a greater pore volume. After the sulfated zirconia was impregnated with heteropolyacid (e.g. an acidic solution of Pd), it was possible for the heteropolyacid to locate at the inner surface of the support pores, resulting in a decrease of pore diameter, as shown in **Table 3**.

3.3. Structure

3.3.1. XRD

The tetragonal and cubic phases of zirconia are of high technological interest in ceramics and catalyst fields. Many studies have shown that only a tetragonal Zr_2O_2 -based catalyst shows good activity for alkane isomerization, while a thermodynamically more stable monoclinic zirconia-based catalyst is completely inactive for alkane isomerization, because one of the necessary conditions for the formation of superacid sites is the existence of metastable tetragonal phase, which may improve the stability of acid sites and acid strength of solid superacids [7]. Many approaches have been reported in attempting to stabilize

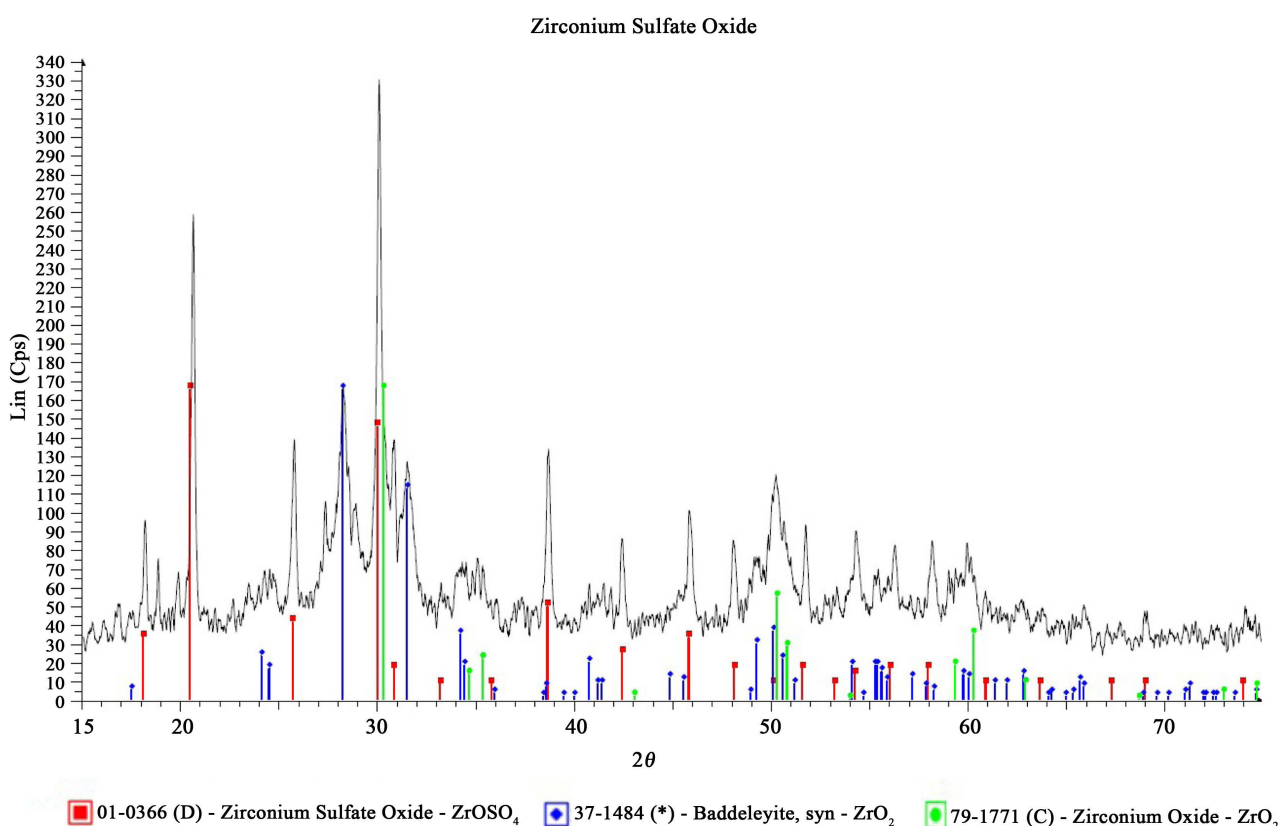


Figure 2. XRD pattern of the sulfated zirconia.

either of these phases at ambient conditions. Most of these approaches include doping with tri-, tetra-, and pentavalent metals or carbonaceous material leading to the formation of oxygen vacancies to achieve charge balance. Oxygen vacancies with trapped electrons favour initial nucleation of tetragonal zirconia, and control the tetragonal-to-monoclinic phase transformation on cooling. Therefore, oxygen ion vacancies are responsible for the stabilization of tetragonal structure of zirconia at low temperature. Recently, however, it has been demonstrated that the stabilization of tetragonal zirconia at low temperature can be achieved also without the addition of the above metals. In addition, it has been shown that precursor anions and OH groups in preparing zirconia can play a complex and important role in the low-temperature stabilization of the tetragonal phase. In the present case, the stabilization of the tetragonal zirconia is mainly controlled by the presence of anion additive such as sulfate.

It is well known that surface sites, which adsorb oxygen at low temperature, are responsible for causing the tetragonal phase to undergo monoclinic transformation at low temperature; in contrast, the incorporation of sulfate covers these sites, retards the formation of larger crystallites of zirconia due to sulfate ions strong effect to attract electrons, and stabilizes tetragonal crystalline phase by retarding the tetragonal-to-monoclinic transformation. It is, in the present case, obvious from **Figure 2** that a predominantly tetragonal structure is stabilized by sulfate. The sulfated zirconia with 8 - 10 nm crystallite is derived from a zirconium oxy-hydroxyl acetate doped by sulphur species at a temperature as high as 650 °C. The d-spacing associated with the diffraction peak at $2\theta = 30.4^\circ$ is 0.294 nm, which is in good agreement with the expected d-spacing of (111) tetragonal zirconia ($d = 0.295$ nm).

The XRD pattern (see **Figure S1** in Supporting Information) of the monometallic Pd-promoted sulphated zirconia. *i.e.*, catalyst reveals formation of zirconium sulfate [$\text{Zr}(\text{SO}_4)_2$] at $2\theta = 20.54^\circ$ and palladium sulphate [PdSO_4] at $2\theta = 24.05^\circ$. XRD measurement of the spent catalyst (see **Figure S2** in Supporting Information) doesn't reveal significant structural changes compared to diffraction pattern of the fresh catalyst, indicating that the composition and structural integrity of the catalyst are not disturbed during the isomerization runs and hence it can be repeatedly used in hexane isomerization.

3.3.2. UV-Vis

UV-Vis spectroscopy gives information about the electronic transitions in the different electronic orbitals of a material, and the lattice defects present in it. In addition, the band-gap of a material may be estimated by extrapolating from the UV-Vis absorption spectrum. The optical band gap of the tetragonal zirconia is approximately at 5.1 eV (226 nm), indicating the presence of many lattice defects, probably cation impurity and/or oxygen vacancy. The optical band gap of bulk monoclinic zirconia is at around 5.2 (240 nm) and 5.7 eV, indicating less defective lattice. Therefore, this observation is complementary to the XRD result where stabilization of tetragonal phase is observed.

The diffuse reflection spectrum shows a high reflection in the visible region and a strong absorption only in the UV part (*i.e.*, <290 nm). The drop in the UV part of reflection curve represents the host lattice absorption from the valence to conduction bands. Zirconia is an insulator material which shows interband transition in the UV region (220 nm) of the electronic spectrum corresponding to the O^{2-} (2p) \rightarrow Zr^{4+} (4d) transition, *i.e.*, ligand-to-metal charge transfer [14].

Figure 3 presents UV-Vis spectrum of our sulfated zirconia, showing an absorption band due to the electronic transition from the valence band to the conduction band. The strong absorption band maximum is centralized at 225 nm for the sulfated zirconia, indicating the presence of tetragonal phase in the sulfated zirconia because the intrinsic absorption of tetragonal zirconia is at 226 nm, as indicated above.

3.3.3. FESEM

A role played by the morphology of the catalyst on catalytic conversion can't be totally excluded. It is, therefore, important to characterize the catalyst by FESEM. The SEM micrograph of the investigated catalyst at 50,000 \times magnification (**Figure 4**) proves to be a porous structure of the catalyst, which consists of nanometer-size particles with identical morphology, especially quasi-spherical in shape and about 8 nm in size. These particles have aggregated each other, forming mesopores with the size of ca.18 and 12 nm. The value correlates well with the average pore size obtained from nitrogen adsorption data.

3.3.4. HRTEM

Microstructure control is a key issue in materials engineering, because almost all

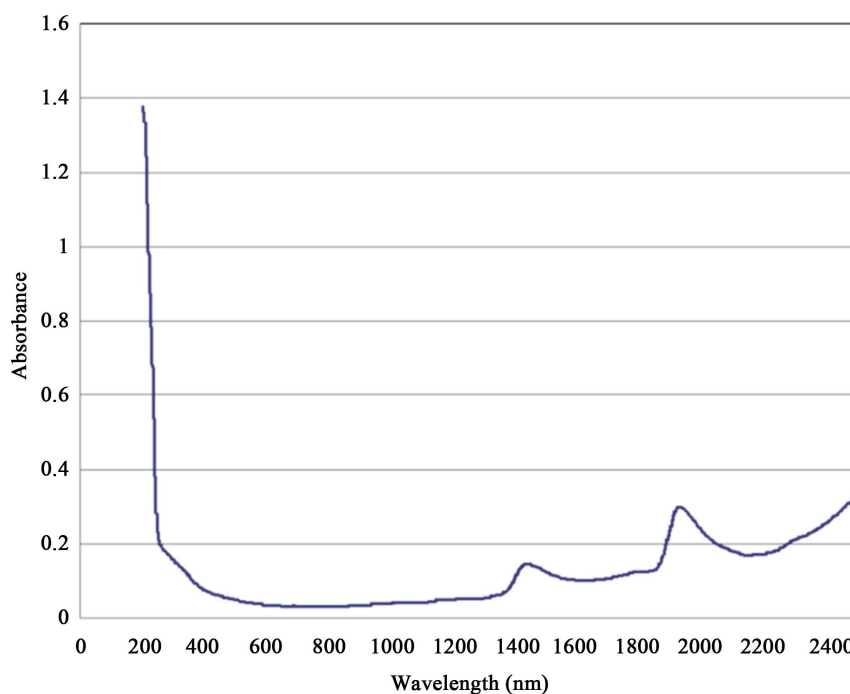


Figure 3. UV-Vis spectrum of the sulfated zirconia.

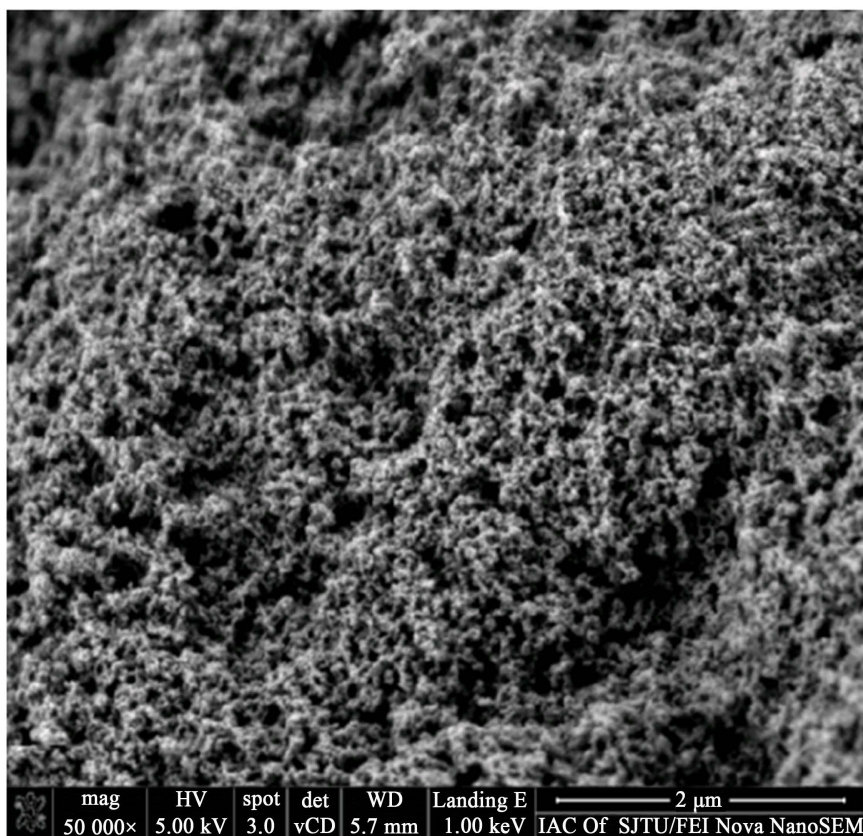
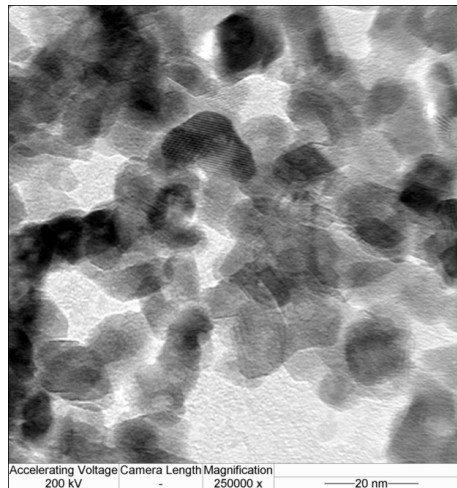


Figure 4. The FESEM image of the catalyst.

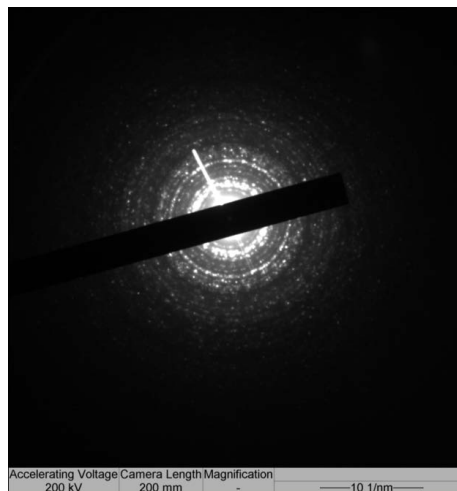
properties depend on internal microstructures. To obtain detailed microstructural information, *i.e.*, the particle size, morphology, agglomeration state, and crystallinity of the sulfated zirconia powder, we performed high-resolution transmission electron microscopy (HRTEM) and selected area electron diffraction (SAED) on the nanostructured catalyst.

In the low magnification TEM image (**Figure 5(a)**), we can clearly observe crystalline nanoparticles with not exactly a spherical or polygonal morphology. The high magnification image shows clear lattice fringes with lattice spacing of 0.315 and 0.284 nm, corresponding to the ($\bar{1}11$) and (111) planes of *m*-ZrO₂, and 0.295 nm that reflects the (111) planes of *t*-ZrO₂. TEM image of the sulfated zirconia reveals that ZrO₂ particles are in nanosize, with their size being ca. 8 nm. The small particle size is advantageous due to shorter diffusion distances for both reaction substrates and products, which increases reaction rates. The high acidity of the sulfated zirconia support could explain the small metal particle size, since the presence of acidic groups increases the hydrophilic character of the support and favors the diffusion of the metal precursor [6].

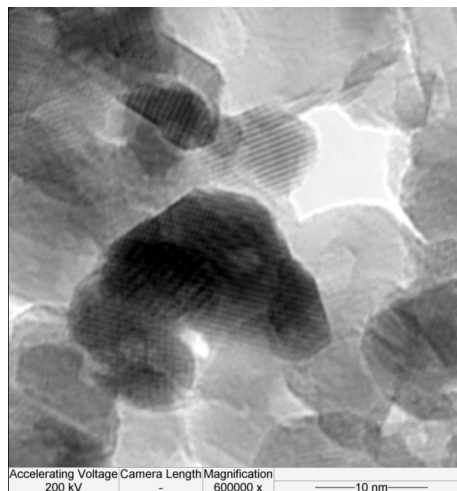
A typical SAED pattern is shown in **Figure 5(b)**. The SAED image confirms that the mesostructured walls are composed of tetragonal phase, displaying characteristic diffuse electron diffraction rings. The diffusive SAED pattern further proves the formation of nanocrystalline zirconia with a tetragonal structure



(a)



(b)



(c)

Figure 5. The characteristic HRTEM images of the catalyst. (a) HRTEM images recorded at lower magnification (250,000); (b) and SAED (selected area electron diffraction); (c) higher magnification (600,000).

because a good match is observed with tetragonal structure, *i.e.*, the obtained tetragonal lattice value was 0.294 nm in agreement with XRD analysis.

3.3.5. XPS

XPS analyses were performed for the samples to verify the presence of sulfate species, determine surface composition especially the S/Zr final molar ratio at the surface and obtain information on the electronic states and chemical environment of carbon, zirconium, oxygen, and sulphur atoms in the catalysts.

Figure 6(d) shows wide-survey XPS spectra in the full range of the binding energy (BE), scanned from 0 to 1200 eV, which provide both a compositional overview and information about main elemental components in the catalyst. The peak for indium (In) originated from the sample mounting. Therefore, it was excluded from the compositional analysis of the samples. XPS beam penetration

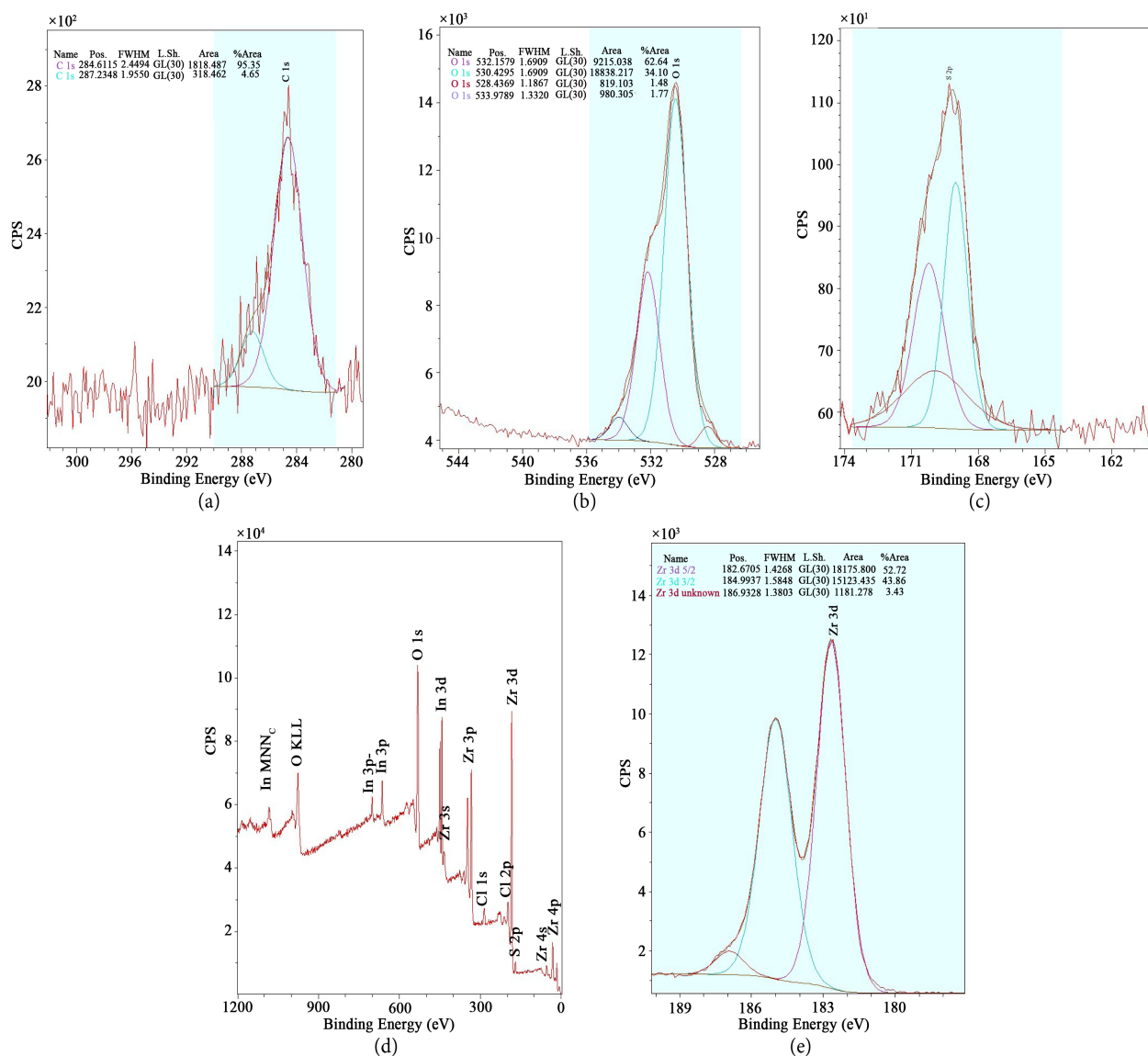


Figure 6. XPS spectra of the catalyst, C 1s (a); O 1s (b); S 2p (c); survey (d); and Zr 3d (e).

corresponds to a thickness that does not exceed 5 nm. Thus, irrespective of the preparation variant, the value (sulphur to zirconium) obtained from XPS measurements exceeds that determined from chemical analysis. **Table 4** presents the surface composition of the fresh and spent catalysts derived from XPS analysis.

The O 1s spectrum (**Figure 6(b)**) for fresh catalyst is the same as that for spent catalyst (**Figure S3** in supporting information), and mainly comprises the first peak at 530.43 eV (fresh) and 530.58 eV (spent), corresponding to the oxygen in the network of zirconia and the second one located at 532.16 eV (fresh) and 531.58 eV (spent) attributed to terminal hydroxyl and sulfate species, showing the binding energy with negligible shift between the fresh and the spent catalyst.

The high resolution scan of C1s region for fresh (**Figure 6(a)**) and spent catalysts (**Figure S3**) shows carbons present in two different chemical environments, corresponding to SP² (C=C) at 284.61 eV (fresh) and 284.87 eV (spent), and the carbonyl (C=O) and alcoholic [C-(OH)] carbon at 287.23 eV (fresh) and 287.20 eV (spent).

Binding energies of sulphur (**Figure 6(c)**) were recorded in the region corresponding to 2p energies. The S 2p peaks located around 169.30 and 170.69 eV for the fresh catalyst and at 169.71 eV for the spent catalyst (**Figure S3**) correspond to a unique sulfated species, resulting in the remarkable acidity on the surface of the sulfated zirconia.

Figure 6(e) depicts the curve fitting in the de-convolution of Zr 3d spectrum for the samples. The main peaks at 185 and 182.67 eV for the fresh catalyst correspond to the Zr 3d_{3/2} and Zr 3d_{5/2}, respectively, which agrees well with the values reported in the literature for ZrO₂ [4].

The accurate P_d superficial concentration is not available due to its low loading and partial overlap of P_d 3d_{5/2} with Zr 3p_{3/2} [14]. Only weak signal exists for the 0.5 wt% P_d catalyst because of the low concentration of P_d atoms [6] [15] [16].

3.3.6. IR

The chemical bonding mode between carboxylic acid, persulfate groups and zirconium centres is elucidated by infrared spectroscopy among the most well-developed analytical techniques for the characterization of organometallic complexes. **Figure 7** presents the infrared spectrum of the pristine complex. The infrared vibrations of the complex are assigned by using evidence from the literature.

Table 4. Surface composition of the fresh and spent catalysts by XPS.

	Zr	O	C	S	S/Zr
Fresh Catalyst (atomic %)	22.4	61.1	13.2	3.3	0.147
Spent Catalyst (atomic %)	22.4	58.2	16.9	2.5	0.111
Fresh Catalyst (weight %)	62.2	29.7	4.8	3.3	0.053
Spent Catalyst (weight %)	62.8	28.6	6.2	2.5	0.04

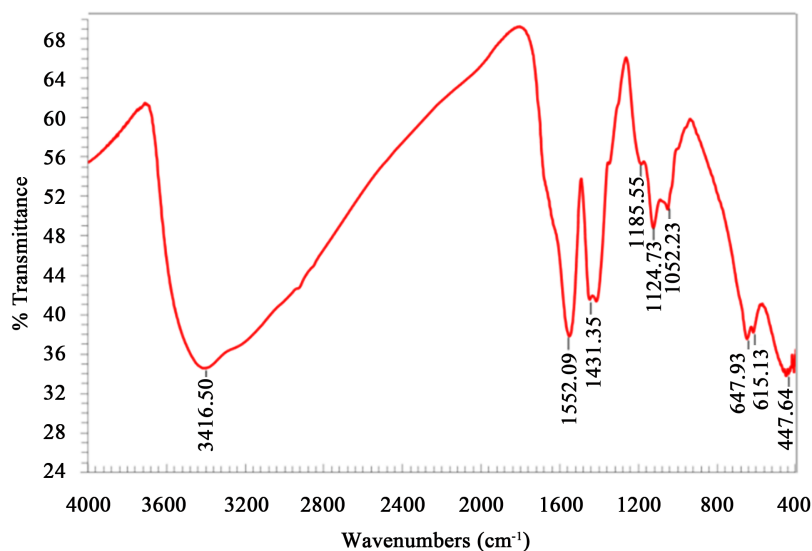


Figure 7. Infrared spectrum of the pristine complex.

The broad band centred around 3416 cm^{-1} is due to the -OH stretching vibration in the acetate and persulfate, and water molecules. The bands around 1552 and 1431 cm^{-1} are ascribed to the asymmetric and symmetric stretching vibrations of the carboxyl (-COO^-) for the acetate ion, respectively. The frequency separation $\Delta\nu$ between the asymmetric and symmetric carboxyl stretching vibrations of an acetate group is an indication of the coordination mode of the acetate ion coordinated to a metal cation [19]. In general, a bidentate bridging acetate complex exhibits a $\Delta\nu$ value less than, but close to, the free ionic value of 160 cm^{-1} . A bidentate chelating acetate complex has $\Delta\nu$ value significantly less than the ionic value, while unidentate coordination results in $\Delta\nu$ value much greater than the ionic value. In the present case, the frequency separation is 121 cm^{-1} , suggesting that acetic acid binds to the zirconium centre in a bidentate bridging or chelating fashion.

The infrared spectra of some known zirconium acetates and oxy-hydroxyl-acetates didn't contain any intense band in the stretching frequency region ($900 - 1100\text{ cm}^{-1}$) of most of the metal-oxygen double bonds [20], thereby indicating the absence of zirconyl group Zr=O in these acetates. The infrared spectrum of the complex under investigation does not exhibit any intense band in $900 - 1100\text{ cm}^{-1}$, and hence there is no formation of Zr=O bond in the complex. An ambiguous and weak band at 1051 cm^{-1} is observed and ascribed to CH_3 rocking [19] or S-O bond vibration [21]-[26] of $\text{S}_2\text{O}_7^{2-}$, *i.e.*, chelating bidentate sulfate and sulfite ions coordinated to zirconium cation. The band at 1051 cm^{-1} remains present even in the complex calcined at 650°C , and therefore should be attributed to S-O bond vibration of $\text{S}_2\text{O}_7^{2-}$. Further, the assignment for the band can be supported by taking into consideration that previous paper [20] that reported the stretching frequencies of metal-oxygen double bonds did not deal with zirconium and that several published works on some zirconium compounds have shown the stretching frequencies of the Zr=O bond at 877 [27] [28] and around

780 cm^{-1} [29] [30].

The bands at 1185 and 1124 cm^{-1} may be assigned to asymmetric and symmetric stretching frequencies of S=O and S-O bonds of $\text{S}_2\text{O}_7^{2-}$, in other words, are typical bands for chelating bidentate sulphate and sulphite ions coordinated to zirconium cation [22] [24] [26] [27].

On the basis of the infrared band assignments of zirconium acetate, oxy-hydroxyl acetate, related carboxylates, oxy-chloride, zirconia, and other metal carboxylates [19] [31], we associate the band at 615 and 647 cm^{-1} with a deformation mode of acetate group rather than sulfate ions. Sulfate anion can form strong complexes with zirconium ion, and the above bands may account for the presence of covalently bound sulfate ions. However, the above bands in the present study almost disappeared as soon as the complex was heated to 400°C, and hence it is attributed to a deformation mode of acetate group rather than sulfate ions.

Overall, it can be assumed from the presence of these infrared bands that the complex is a sulphur species-doped zirconium oxy-hydroxyl acetate complex in which an acetate ion is directly bonded to the zirconium of zirconium tetramer mainly in a chelating bidentate coordination mode and the resulting tetramers are linked together by acetate or persulfate ions.

On the basis of the above infrared spectrum of the pristine complex, we can easily understand the infrared spectra of the sulfated zirconia, Pd-promoted sulfated zirconia and spent catalyst. As shown in **Figure 8**, a broad peak at 3427 cm^{-1} corresponds to the hydroxo- and aquo-OH stretching vibrations of hydroxyl groups, and adsorbed water is accompanied by the band at 1632 cm^{-1} [9] [32]. The weak bands at 2925 cm^{-1} can be assigned to the bending/scissoring and stretching vibration of C-H and CH_3 groups [9] [33] [34].

The surface sulphur species are present in sulfated zirconia most likely in the form of pyrosulphate species showing a characteristic IR band around 1401 cm^{-1} , which should be responsible for the high catalytic acidity in the acid-catalysed reactions. In the pyrosulphate species Zr atoms are directly coordinated to strongly electron-withdrawing SO_x centres. This configuration shows the characteristic asymmetric and symmetric stretching frequencies of partially ionized S=O double bonds and S-O bonds in the region of 1200 - 900 cm^{-1} , as shown in infrared spectra.

The peaks at 1140, 1052 cm^{-1} , characteristic of inorganic chelating bidentate sulfate ion coordinated to metal cations (Zr^{4+}), are assigned to asymmetric and symmetric stretching frequencies of S=O and S-O bonds, indicating that the impregnation of persulfate ions on the surface of zirconia was in bidentate fashion [9] [34] [35]. It is, therefore, obvious that the superacidity of the catalyst studied may be attributed to the presence of zirconium-bound sulfate groups. The IR bands at 749 and 589 cm^{-1} are attributed to Zr-O stretching modes, characteristic of crystalline zirconia. Finally, it can be clearly known from **Figure 8** that the infrared spectrum of the spent catalyst is similar to that observed for the fresh catalyst.

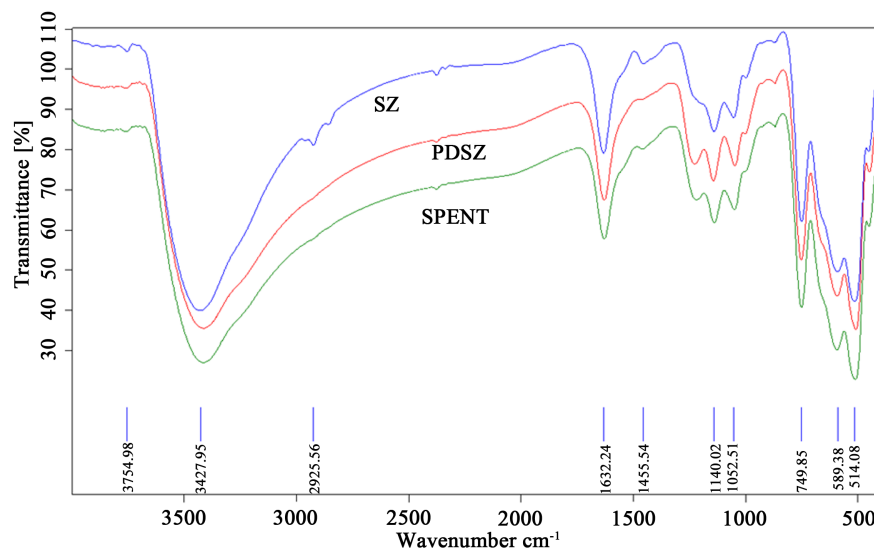


Figure 8. Infrared spectra of the sulfated zirconia (SZ), Pd-promoted sulfated zirconia (Pd-SZ), and spent catalyst.

3.3.7. TG-MS

Investigation of the thermal behaviour of the complex may be conducive in clarifying the composition and structure of the complex synthesized by the present process. Thermogravimetric (TG), differential scanning calorimetry (DSC) and elemental analyses were used to obtain information about the thermal behaviour of the complex when it was heated in air.

When the complex was heated up to 800°C in air, the TG and DSC traces are shown in **Figure 9**. It can be seen that a one-to-one correlation exists between the DSC and TG traces, indicating that the thermal effects are accompanied by weight losses. The complex is found to decompose to zirconia in three steps, as shown in the DSC curve: one endothermic and two exothermic decomposition processes. The endothermic event occurs around 91°C and originates from the dehydration (physisorbed H₂O) of the dried precipitating complex, with a corresponding weight loss being about 9.41%, as indicated in the TG curve. It may be noted from the DSC curve that after dehydration there are two exothermic peaks, centred around 376°C and 546°C, respectively. It has been noted that liberation of chemisorbed H₂O takes place between 300°C and 500°C [36]. The corresponding weight loss for the two exothermic steps, as estimated from the TG curve, are 13.87% and 1.96%, respectively, suggesting that most of the complex should be decomposed in the first exothermic step.

The EDXS analysis (wt%) of the pristine complex reveals Zr (54.85), Hf (1.44), C (16.27), O (27.11), and S (0.33) present in it. It has been accepted that EDXS analysis is not sensitive to the determination of non-metals, and that metals may be more accurately determined by ICP-IES than by EDXS. Therefore, based on the clue given by the EDXS analysis, we have quantitatively determined the metal and non-metals by ICP-AES and by elemental analysis and X-ray fluorescence spectroscopy, respectively, yielding (wt%) Zr (51.85), S (2.388), H (3.15), N (0),

and Cl (0). Combined with the data derived from the thermal gravimetric and elemental analyses, the pristine complex can be represented by an empirical formula: $Zr_4(S_2O_7)_{0.25}O_2(OH)_5(CH_3COO)_6 \cdot H_2O$.

Figure 10 shows the ion current curve for evolved gases in the TG-MS measurement of the catalyst. As shown in **Figure 10**, water vapor is the evolved gas from 90°C to 350°C. Carbon dioxide, carbon monoxide, and methyl oxide (CH_3O) occur over ~380°C, 450°C, and 400°C, respectively. No evolution of SO , SO_2 and SO_3 is found during the evolved gas analysis, suggesting a good thermal stability of the sulfated zirconia catalyst. The weight loss below 620°C from TG

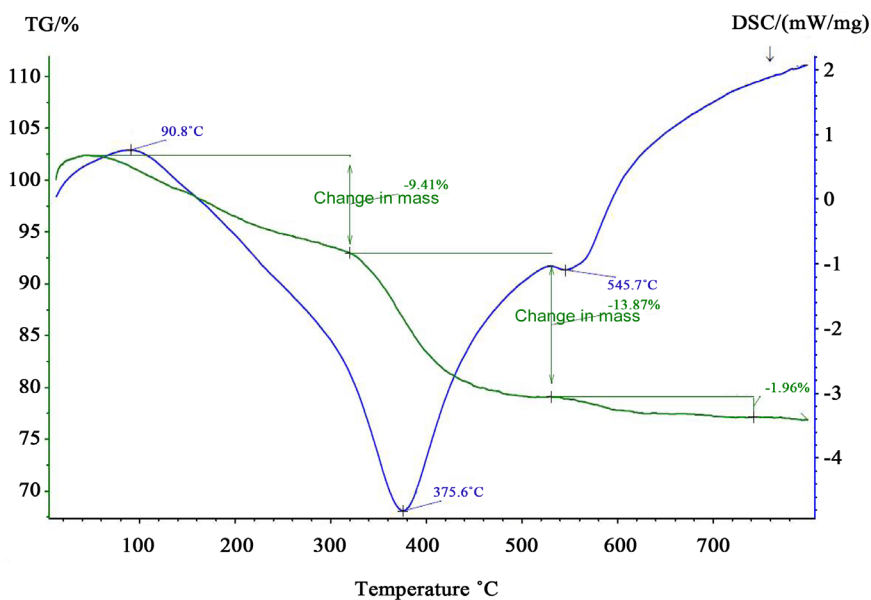


Figure 9. DSC and TG curves of the pristine complex.

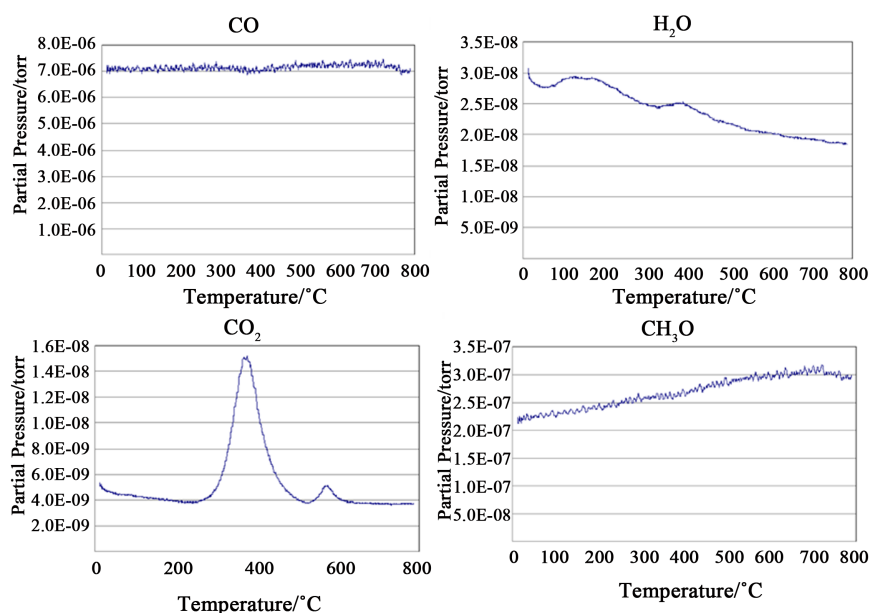


Figure 10. Evolved gases CO , H_2O , CO_2 and CH_3O in TG-MS measurements.

analysis is attributed to elimination of adsorbed water and oxidation of carbon, It is, therefore, clear, from the IR and TG-MS data that the superacidity of the catalyst studied may be attributed to the presence of stable zirconium-bound sulfate groups.

4. Conclusions

This article elucidates the reason why mesoporous sulfated zirconia can be prepared under structure-directing-free at 650 °C from zirconyl chloride, acetic acid and ammonium persulfate system.

According to the acidity measurement, it is worth pointing out that the typical Brønsted acidities (1540 and 1638 cm^{-1}) for the catalyst, *i.e.*, monometallic Pd-promoted sulphated zirconia (Table 2) can be interesting strengthened by raising temperature, leading to a high catalytic activity in n-hexane isomerization.

It is shown from nitrogen adsorption and desorption measurement that pronounced desorption hysteresis is present in the isotherm, indicating the presence of large mesopores in the catalyst.

The XRD patterns demonstrate that the Pd-promoted sulfated zirconia is a nearly pure tetragonal zirconia with 8 - 10 nm crystallite, which is supported by UV-VIS spectroscopy.

HRTEM images show that particles are faceted single crystals with not exactly a spherical but much more of a polygonal shape and with clear lattice fringes corresponding to crystallographic planes of the tetragonal zirconia, due to the interplanar spacing (0.294 nm) being in agreement with the d-spacing (0.295 nm) of the (111) plane of tetragonal zirconia.

XPS analyses were performed for the samples to verify the presence of sulfate species, determine surface composition especially the S/Zr final molar ratio at the surface and obtain information on the electronic states and chemical environment of carbon, zirconium, oxygen, and sulphur atoms in the catalysts.

It is clear from TG-MS, ICP-AES, and IR analyses that the precursor of the catalyst is a sulphur species-doped zirconium oxy-hydroxyl acetate complex. The superacidity of the catalyst studied may be associated with the presence of zirconium-bound sulfate groups. The sulfated zirconia catalyst possesses a good thermal stability.

Acknowledgements

We are grateful to Dr. Manager Director Jicang Guo at Guy Carpenter & Company Pty Ltd. for assistance in preparing Figure s and tables.

Conflicts of Interest

The authors declare no competing financial interest.

References

- [1] Schmidt, W.D.G., Pichler, C.M., Bongard, H.J., Spliethoff, B.S., Asahina, S., Cao, Z., Terasaki, O. and Schgth, F. (2017) Surface-Casting Synthesis of Mesoporous Zirco-

- nia with a CMK-5-Like Structure and High Surface Area. *Angewandte Chemie International Edition*, **56**, 11222-111225. <https://doi.org/10.1002/anie.201705042>
- [2] Pastvova, J., Dalibor Kaucy, D., Moravkova, J., Rathousky, J., Sklenak, S., Vorokhta, M., Brabec, L., Pilar, R., Jakubec, I., Tabor, E., Klein, P. and Szama, P. (2017) Effect of Enhanced Accessibility of Acid Sites in Micromesoporous Mordenite Zeolites on Hydroisomerization of n-Hexane. *ACS Catalysis*, **7**, 5781-5795. <https://doi.org/10.1021/acscatal.7b01696>
- [3] Guo, G.Y., Chen, Y.L. and Xu, S. (2015) A Luminescent Mesoporous Zirconium Complex and It as a Precursor of Environmentally Benign Catalysts. *Microporous and Mesoporous Materials*, **213**, 100-107. <https://doi.org/10.1016/j.micromeso.2015.04.013>
- [4] John, F.M., Stickle, W.F. and Sobol, P.E. (1992) Handbook of X-Ray Photoelectron Spectroscopy. Perkin-Elmer Corporation, Physical Electron Division.
- [5] Perras, F.A., Wang, Z., Naik, P. and Slowing, I. (2017) Natural Abundance 17O DNP NMR Provides Precise O-H Distances and Insights into the Brønsted Acidity of Heterogeneous Catalysts. *Angewandte Chemie International Edition*, **56**, 9165-9169. <https://doi.org/10.1002/anie.201704032>
- [6] Bedia, J., Arevalo-Bastanta, J.M.G., Dosso, L.A., Rodriguez, J.J., Mayoral, I.D. and Gmez-Sainero, I.M. (2017) Effect of the Pt-Pd Molar Ratio in Bimetallic Catalysts Supported on Sulfated Zirconia on the Gas-Phase Hydrodechlorination of Chloromethanes. *Journal of Catalysis*, **352**, 562-571. <https://doi.org/10.1016/j.jcat.2017.06.013>
- [7] Wang, P., Zhang, J., Wang, G., Li, C. and Yang, C. (2016) Nature of Active Sites and Deactivation Mechanism for n-Butane Isomerization over Alumina-Promoted Sulfated Zirconia. *Journal of Catalysis*, **338**, 124-134. <https://doi.org/10.1016/j.jcat.2016.02.027>
- [8] Sing, K.S.W., Everett, D.H., Haul, R.A.W., Moscou, L. and Pierotti, R.A. (1985) Reporting Physisorption Data for Gas/Solid Systems with Special Reference to the Determination of Surface Area and Porosity. IUPAC Commission on Colloid and Surface Chemistry Including Catalysis. *Pure and Applied Chemistry*, **57**, 603-619.
- [9] Banerjee, B., Bhunia, S. and Bhaumik, A. (2015) Self-Assembled Sulfated Zirconia Nanocrystals with Mesoscopic Void Space Synthesized via Ionic Liquid as a Porogen and Its Catalytic Activity for the Synthesis of Biodiesels. *Applied Catalysis A: General*, **502**, 380-387. <https://doi.org/10.1016/j.apcata.2015.06.028>
- [10] Zhang, X., Johnson, J.A., Chen, Y.S. and Zhang, J. (2016) Highly Porous Zirconium Metal-Organic Frameworks with β -UH3-Like Topology Based on Elongated Tetrahedral Linkers. *Journal of the American Chemical Society*, **138**, 8380-8383. <https://doi.org/10.1021/jacs.6b04608>
- [11] Deria, P., Goaf-Gualdron, D.A., Hod, I., Snurr, R.Q., Hupp, J.T. and Farha, O.K. (2016) Framework-Topology-Dependent Catalytic Activity of Zirconium-Based (Porphinato)zinc(II) MOFs. *Journal of the American Chemical Society*, **138**, 14449-14457. <https://doi.org/10.1021/jacs.6b09113>
- [12] Wang, T.C., Bury, W., Gomez-Gualdron, D.A., Vermeulen, N.A., Mondloch, J.E., Deria, P., Zhang, K., Moghadam, P.Z., Sarjeant A.A., Snurr, R.Q., Stoddart, J.F., Hupp, J.T. and Farha, O.K. (2015) Ultrahigh Surface Area Zirconium MOFs and Insights into the Applicability of the BET Theory. *Journal of the American Chemical Society*, **137**, 3585-3591. <https://doi.org/10.1021/ja512973b>
- [13] Feng, D., Wang, K., Su, J., Liu, T.-F., Park, J., Wei, Z., Bosch, M., Yakovenko, A., Zou, X. and Zhou, H.-C. (2015) A Highly Stable Zeotype Mesoporous Zirconium

- Metal-Organic Framework with Ultralarge Pores. *Angewandte Chemie International Edition*, **54**, 149-154. <https://doi.org/10.1002/anie.201409334>
- [14] Han, Y., Sun, J., Fu, H., Qu, X., Wan, H., Xu, Z. and Zheng, S. (2016) Highly Selective Hydrodechlorination of 1,2-Dichloroethane to Ethylene over Ag-Pd/ZrO₂ Catalysts with Trace Pd. *Applied Catalysis A: General*, **519**, 1-6. <https://doi.org/10.1016/j.apcata.2016.03.017>
- [15] Tian, P., Quyang, L., Xu, X., Ao, C., Xu, X., Si, R., Shen, X., Lin, M., Xu, J. and Han, Y.-F. (2017) The Origin of Palladium Particle Size Effects in the Direct Synthesis of H₂O₂: Is Smaller Better? *Journal of Catalysis*, **349**, 30-40. <https://doi.org/10.1016/j.jcat.2016.12.004>
- [16] Pino, N., Sitthisa, S., Tan, Q., Souza, T., Lopez, D., Daniel, E. and Resasco, D.E. (2017) Structure, Activity, and Selectivity of Bimetallic Pd-Fe/SiO₂ and Pd-Fe/ γ -Al₂O₃ Catalysts for the Conversion of Furfural. *Journal of Catalysis*, **350**, 30-40. <https://doi.org/10.1016/j.jcat.2017.03.016>
- [17] Wang, H., Chen, H., Ni, B., Wang, K., He, T., Wu, Y. and Wang, X. (2017) Mesoporous ZrO₂ Nanoframes for Biomass Upgrading. *ACS Applied Materials & Interfaces*, **9**, 26897-26906. <https://doi.org/10.1021/acsami.7b07567>
- [18] Wang, P., Feng, J., Zhao, Y., Wang, S. and Liu, J. (2016) MOF-Derived Tungstated Zirconia as Strong Solid Acids toward High Catalytic Performance for Acetalization. *ACS Applied Materials & Interfaces*, **8**, 23755-23762. <https://doi.org/10.1021/acsami.6b08057>
- [19] Nakamoto, K. (1997) Infrared and Raman Spectra of Inorganic and Coordination Compounds Part B. 5th Edition, Wiley & Sons Inc., New York.
- [20] Barraclough, C.G., Lewis, J. and Nyholm, R.S. (1959) The Stretching Frequencies of Metal-Oxygen Double Bonds. *Journal of the Chemical Society*, **11**, 3552-3555. <https://doi.org/10.1039/JR9590003552>
- [21] Klose, B.S., Jentoft, F.C. and Schlogl, R. (2005) *In Situ* Diffuse-Reflectance Infrared Spectroscopic Investigation of Promoted Sulfated Zirconia Catalysts during n-Butane Isomerization. *Journal of Catalysis*, **233**, 68-80. <https://doi.org/10.1016/j.jcat.2005.04.011>
- [22] Li, X., Nagaoka, K., Olindo, R. and Lercher, J.A. (2006) Synthesis of Highly Active Sulfated Zirconia by Sulfation with SO₃. *Journal of Catalysis*, **238**, 39-45. <https://doi.org/10.1016/j.jcat.2005.11.039>
- [23] San, Y., Ma, S., Du, Y., Yuan, L., Wang, S., Yang, J., Deng, F. and Xiao, F.-S. (2005) Solvent-Free Preparation of Nanosized Sulfated Zirconia with Brønsted Acidic Sites from a Simple Calcination. *The Journal of Physical Chemistry*, **109**, 2567-2572. <https://doi.org/10.1021/jp046335a>
- [24] Deshmane, V.G. and Adewuyi, Y.G. (2013) Mesoporous Nanocrystalline Sulfated Zirconia Synthesis and Its Application for FFA Esterification in Oils. *Applied Catalysis A: General*, **462-463**, 196-206. <https://doi.org/10.1016/j.apcata.2013.05.005>
- [25] Marakatti, V.S., Shanbhag, G.V. and Halgeri, A.B. (2013) Sulfated Zirconia; an Efficient and Reusable Acid Catalyst for the Selective Synthesis of 4-phenyl-1,3-dioxane by Prins Cyclization of Styrene. *Applied Catalysis A: General*, **451**, 71-78. <https://doi.org/10.1016/j.apcata.2012.11.016>
- [26] Reddy, B.M. and Patil, M.K. (2009) Organic Syntheses and Transformations Catalyzed by Sulfated Zirconia. *Chemical Reviews*, **109**, 2185-2208. <https://doi.org/10.1021/cr900008m>
- [27] Jana, S. and Biswas, P.K. (1997) Chemical Behaviour of Zirconium Oxychloride Octahydrate and Acetic Acid in Precursor Solution for Zirconia Film Formation on

Glass. *Journal of Sol-Gel Science and Technology*, **9**, 227-237.

<https://doi.org/10.1023/A:1018395509844>

- [28] Cotton, F.A. (1972) *Advanced Inorganic Chemistry*. 3rd Edition, John Wiley & Sons Inc., New York.
- [29] Howard, W.A., Trnka, T.M., Waters, M. and Parkin, G. (1997) Terminal Chalcogenido Complexes of Zirconium: Syntheses and Reactivity of $Cp_2^*Zr(E)(NC_5H_5)$ ($E = O, S, Se, Te$). *Journal of Organometallic Chemistry*, **528**, 95-121.
[https://doi.org/10.1016/S0022-328X\(96\)06584-9](https://doi.org/10.1016/S0022-328X(96)06584-9)
- [30] Pakin, G. and Karlin, K.D. (1998) *Progress in Inorganic Chemistry*. John Wiley & Sons Inc., New York, 10166.
- [31] Colthup, N.B., Daly, L.H. and Wiberley, S.E. (1990) *Introduction to Infrared and Raman Spectroscopy*. 3rd Edition, Academic Press Inc., New York.
- [32] Brusau, E.V., Narda, G.E. and Pedregosa, J.C. (1999) Vibrational and Thermal Evidence of Coordinated Water and Carboxylate Groups in Crystalline Calcium Malonate Dihydrate. *Journal of Solid State Chemistry*, **143**, 174-181.
<https://doi.org/10.1006/jssc.1999.8069>
- [33] Hosseini, M.M., Kolvari, E., Koukabi, N., Ziyaei, M. and Zolfigol, M.A. (2016) Zirconia Sulfuric Acid: An Efficient Heterogeneous Catalyst for the One-Pot Synthesis of 3,4-Dihydropyrimidinones under Solvent-Free Conditions. *Catalysis Letters*, **146**, 1040-1049. <https://doi.org/10.1007/s10562-016-1723-8>
- [34] Vargas, A.D., Mendez, J.L., Canepa, S.A. and Bravo, D.R. (2017) Sulfated Zirconia: An Efficient and Reusable Heterogeneous Catalyst in the Friedel-Crafts Acylation Reaction of 3-Methylindole. *Catalysis Letters*, **147**, 1496-1502.
<https://doi.org/10.1007/s10562-017-2057-x>
- [35] Song, H., Wang, N., Song, H.L. and Li, F. (2015) La-Ni Modified $S_2O_8^{2-}/ZrO_2-Al_2O_3$ Catalyst in n-Pentane Hydroisomerization. *Catalysis Communications*, **59**, 61-64.
<https://doi.org/10.1016/j.catcom.2014.09.037>
- [36] Liu, N., Guo, X., Navrotsky, A., Shi, L. and Wu, D. (2016) Thermodynamic Complexity of Sulfated Zirconia Catalysts. *Journal of Catalysis*, **342**, 158-163.
<https://doi.org/10.1016/j.jcat.2016.08.001>

Supporting Information

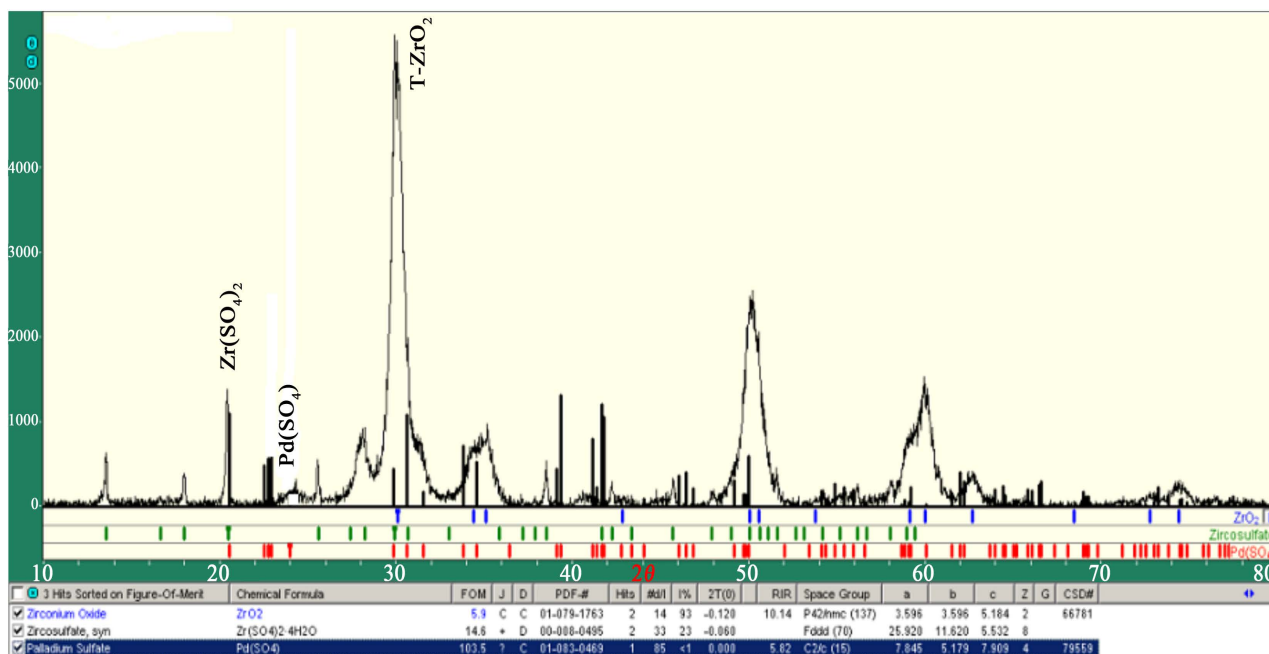


Figure S1. XRD pattern of monometallic Pd-promoted sulfated zirconia.

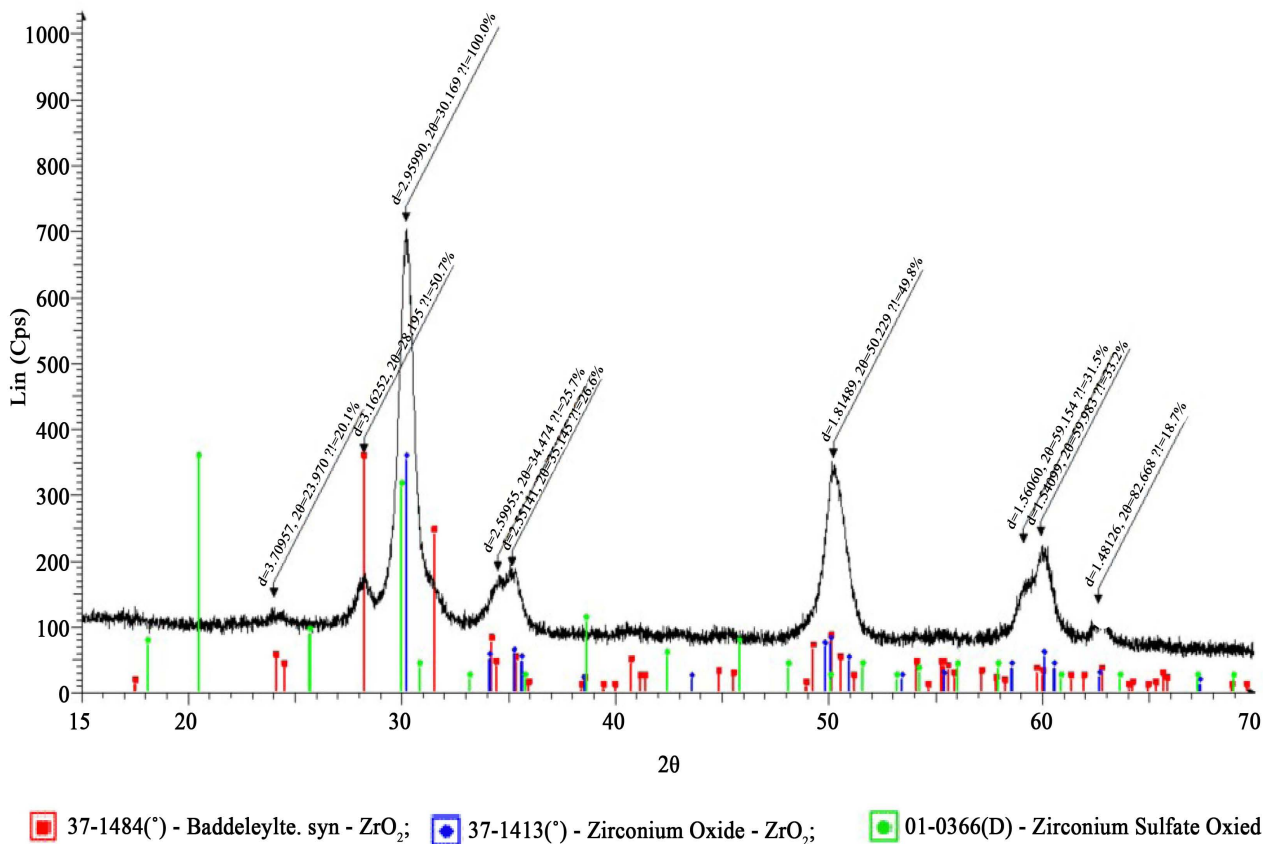


Figure S2. XRD pattern of the spent catalyst.

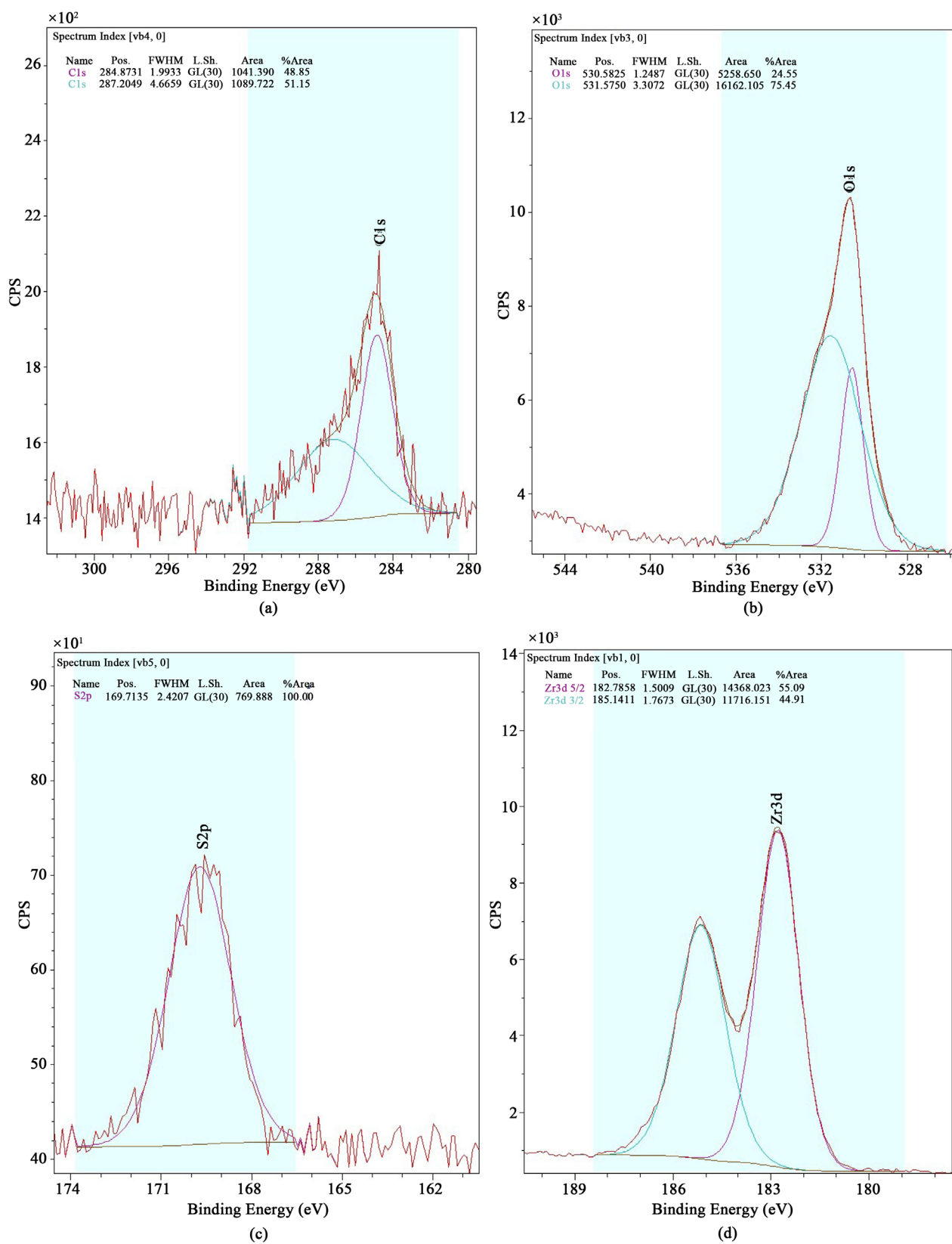


Figure S3. The XPS spectra of the spent catalyst, C1s (a); O1s (b); S2p (c) and Zr3d (d).